Double NPY motifs at the N-terminus of Sso2 synergistically bind Sec3 to promote membrane fusion

Maximilian Peer[1,3], Hua Yuan[2,3], Yubo Zhang[1,3,4], Katharina Korbula[1], Peter J. Novick[2,*], Gang Dong[1,*]

[1]Max Perutz Labs, Vienna Biocenter, Medical University of Vienna, 1030 Vienna, Austria

[2]Department of Cellular and Molecular Medicine, University of California San Diego, La Jolla, CA 92093, USA

[3]These authors contributed equally

[4]Current address: Foshan University, Guangdong Province 528000, China

[*]Correspondence: pnovick@ucsd.edu (P.J.N.), gang.dong@meduniwien.ac.at (G.D.)

Keywords: exocyst; membrane fusion; Sec3; SNARE; Sso2

Abstract

Exocytosis is an active vesicle trafficking process by which eukaryotes secrete materials to the extracellular environment and insert membrane proteins into the plasma membrane. The final step of exocytosis in yeast involves the assembly of two t-SNAREs, Sso1/2 and Sec9, with the v-SNARE, Snc1/2, on secretory vesicles. The rate-limiting step in this process is the formation of a binary complex of the two t-SNAREs. Despite of the previous report for how the binary complex assembly is accelerated by Sec3, it remains unknown how Sso2 is efficiently recruited to the vesicle-docking site marked by Sec3. Here we report a crystal structure of the pleckstrin homology (PH) domain of Sec3 in complex with a nearly full-length version of Sso2 only lacking its C-terminal transmembrane helix. The structure shows an uncharacterized binding site for Sec3 at the N-terminus of Sso2, consisting of two highly conserved triple residue motifs (NPY: Asn-Pro-Tyr). We further reveal that the two NPY motifs bind Sec3 synergistically and play an essential role in the fusion of secretory vesicles at target sites on the plasma membrane.

Significance

SNARE assembly, which involves one v-SNARE with two t-SNARE proteins, drives the fusion of vesicles to target compartments. The rate-limiting step in SNARE assembly is the assembly of the two t-SNARE proteins on the target membrane. Previous studies showed that in yeast Sec3, a component of the exocyst vesicle tethering complex, directly interacts with the t-SNARE protein Sso2 to promote fast assembly of an Sso2-Sec9 binary t-SNARE complex. This paper presents a new crystal structure of the Sec3 PH domain in complex with a nearly full-length version of Sso2, which reveals a previously unknown binding site for Sec3 at the N-terminus of Sso2. Our work demonstrates that the interaction between Sso2 and Sec3 plays an essential role in promoting the fusion of secretory vesicles at target sites on the plasma membrane.

Introduction

The cytoplasm in eukaryotic cells is compartmentalized into distinct membrane bound organelles. Inter-organelle material exchange is carried out primarily through membrane traffic in which membrane bound transport vesicles bud from a donor compartment and are delivered to a specific acceptor compartment. Upon arriving at the destination, cargo-packed vesicles are first recognized and caught by tethering factors situated on the target membrane, which then hand the captured vesicles over to the soluble N-ethylmaleimide-sensitive factor-attachment protein receptor (SNARE) proteins that drive membrane fusion [1-4].

There are several types of SNARE proteins, one of which is attached to the membrane of vesicles (v-SNARE), and the others are on the target membrane (t-SNARE). In neuronal exocytosis, fusion of synaptic vesicles to the presynaptic plasma membrane is driven by the assembly of a four-helix bundle containing two t-SNAREs, syntaxin-1 and SNAP-25, on the target membrane and the v-SNARE, synaptobrevin, on synaptic vesicles [5, 6]. Extensive studies have established that SNARE assembly is tightly regulated by multiple auxiliary proteins, including the Sec1/Munc18 (SM) family of proteins, tethering factors, and small GTPases [7-12]. Munc18 is a chaperone protein that maintains syntaxin-1 in an activated conformation and passes it to its cognate SNARE partners for assembly to catalyze membrane fusion [13-17].

The exocytic vesicle-docking site in yeast is marked by the octameric exocyst complex, which belongs to the CATCHR family of multi-subunit tethering proteins [18-20]. The main function of the exocyst is to capture secretory vesicles at sites of cell surface growth, which include the tip of the daughter cell early in the cell cycle, and the mother-

daughter cell junction late in the cycle [21]. The two t-SNAREs for exocytosis in yeast are Sso1/2 and Sec9, which are homologs of syntaxin-1 and SNAP-25, respectively. The v-SNARE attached to secretory vesicles in yeast is Snc1/2, which is equivalent to synaptobrevin in neuronal exocytosis.

Our previous work showed that one of the exocyst components, Sec3, promotes SNARE assembly by interacting with the t-SNARE Sso2 [22]. Sec3 consists of an N-terminal pleckstrin homology (PH) domain, a central putative coiled coil, and a C-terminal helical domain. Like syntaxin-1 and other related t-SNAREs, Sso2 consists of four helices, with the first three (Habc) forming an inhibitory domain and the last (H3) serving as the SNARE motif that interacts with the other two SNAREs during membrane fusion. We have shown that the Sec3 PH domain binds to the auto-inhibited four-helix bundle of Sso2 and promotes a conformational change of the linker between Hc and H3 of Sso2 via an allosteric effect. This change promotes the release of the SNARE motif (H3) of Sso2 and substantially accelerates the formation of the initial binary complex between H3 of Sso2 and the two helices of the other t-SNARE, Sec9. However, it remains unclear how Sso2 is initially recruited to the vesicle target sites marked by the exocyst to drive the efficient fusion reaction between secretory vesicles and the plasma membrane.

Here we report structural studies of Sec3-PH in complex with a nearly full-length construct of Sso2 (aa1-270), which lacks only its C-terminal transmembrane region (aa271-295). Our crystal structure of this Sec3/Sso2 complex reveals a previously unknown binding site for Sec3 on Sso2 in addition to the one on its four-helix bundle as reported in our previous work [22]. This extra binding site is located at the N-terminal end of Sso2 and consists of two highly conserved NPY (i.e. Asn-Pro-Tyr) motifs. These NPY

motifs are connected to the helical core of Sso2 (i.e. Habc and H3) via a long variable linker. In the two heterodimeric complexes present in the crystal structure, the two NPY motifs of the two Sso2 molecules bind individually to a similar conserved hydrophobic pocket on the two Sec3 molecules. Interestingly, however, our *in vitro* interaction studies using synthetic polypeptides and recombinant Sec3-PH protein demonstrated that each NPY motif alone bound Sec3 much more weakly than the two NPY motifs together. The importance of the interaction between the NPY motifs of Sso2 and Sec3 was confirmed by a series of *in vivo* assays in yeast.

Overall, our work has uncovered a new interaction interface between Sec3 and Sso2, which suggests an extra regulatory step in exocytic membrane fusion. Binding of the NPY motifs of Sso2 allows efficient recruitment of the t-SNARE protein to the vesicle-docking site on the plasma membrane to facilitate vesicle fusion.

Results

Crystal structure reveals two NPY motifs at the N-terminus of Sso2 bound individually to Sec3-PH domain

We previously reported the structure of Sso2-HabcH3 (aa36-227) in complex with the PH domain of Sec3 (aa75-320)[22]. We subsequently crystallized another complex of the two proteins using a longer version of Sso2 (aa1-270), which contains all Sso2 sequence except for its C-terminal transmembrane part, together with a shorter Sec3-PH domain (aa75-260) (**Fig. 1A** and **Fig. S1A**). A stable binary complex was obtained via size exclusion chromatography (SEC) (**Fig. S1B**), which was then crystallized by hanging

drop vapor diffusion. Diffraction data to 2.19 Å resolution was collected at the ESRF and the crystal structure was determined by the molecular replacement method. The crystal belongs to space group *P*1 (a = 50.96 Å, b = 58.40 Å, c = 83.29 Å; α = 104.28°, β = 98.49°, γ = 113.20°). The final structure was refined to R_{work} and R_{free} of 19.9% and 23.9%, respectively, with an average B factor of 40.74 $Å^2$ for all macromolecules (**Table 1**).

The final model contains two copies of the Sso2-Sec3 complex per asymmetric unit, together with 418 ordered water molecules. One of the complexes contains residues 4-8, 33-149 and 197-226 of Sso2 and residues 76-250 of Sec3; the other contains residues 6-14, 33-148 and 196-226 of Sso2 and residues 76-250 of Sec3. Corresponding regions in the two complex structures are essentially identical, with r.m.s.d of 0.45 Å for all aligned backbone atoms (**Fig. 1B**). $2F_o$-F_c electron density maps have a high quality, and sidechains of most residues in both Sec3 and Sso2 can be confidently built (**Fig. 1C**).

Primary sequence alignments of Sso2 homologs from various yeast species reveal two conserved three-residue motifs toward the N-terminus of Sso2, which we name as NPY motifs. These double NPY motifs are connected to the highly conserved core of Sso2 (i.e. Habc and H3) via a nonconserved linker with variable lengths in different homologs (**Fig. 2A** and **Fig. S2**). These NPY motifs bind individually to Sec3 in the two structural copies (**Fig. 2 B** and **E**). In one complex structure residues 4-8 of Sso2 show clear densities in the $2F_o$-F_c map (**Fig. 2C**); in the other structure we could unambiguously trace sidechains of residues 10-14, but for residues 6-9 we could build only the backbone atoms (**Fig. 2F**). Despite variations in the flanking residues of these NPY motifs, the NPY cores adopt essentially the same conformation and share similar contacts with ordered solvent molecules and neighboring residues from Sec3 (**Fig. S3**). Particularly, the tyrosine

residues (i.e. Y7 and Y13) in both cases are docked into a conserved hydrophobic pocket on the concave surface on Sec3 (**Fig. 2 D** and **G**). Overall, the NPY motif adopts a T-shaped conformation, with its broad top part shaped by the asparagine (N) and the proline (P) residues, which is stabilized by a hydrogen bond between the carboxyal group of the asparagine and the amide proton of the proline (**Fig. 2H**). The tryosine residue sticks out to form a pin-like structure that fits neatly in the pocket on Sec3.

The two NPY motifs of Sso2 binds synergistically to Sec3

To determine how the two NPY motifs of Sso2 interact with Sec3, we carried out isothermal titration calorimetry (ITC) assays using synthetic polypeptides of Sso2 and recombinant Sec3 protein purified from bacteria (**Fig. 3**). Wild type (WT) double NPY motifs of Sso2 (aa1-15) bound Sec3 with a dissociation constant (K_d) of 21.1 µM (**Fig. 3A**). However, each NPY motif individually bound Sec3 much more weakly, with K_d values increased by 3-4 fold (**Fig. 3 B** and **C**). Mutation of core residues of the first NPY motif to alanines (M5) slightly reduced the binding affinity (K_d = 34.9 µM) (**Fig. 3D**), whereas that of the second NPY motif (M6) drastically affected the interaction, with a K_d of 188 µM (**Fig. 3E**). The synthetic polypeptide with both NPY motifs mutated (M7) displayed no detectable interaction with Sec3 (**Fig. 3F**).

Mutation of Sso2 NPY motifs inhibits cell growth as well as secretion of Bgl2 and invertase

To assess the *in vivo* role of the interactions between Sec3 and the two NPY motifs of Sso2, we constructed various *sso2* alanine substitution mutations in a yeast integrating vector and introduced them into a yeast strain deleted for the paralogous gene, *SSO1.* The mutations were incorporated into the endogenous *SSO2* locus by the loop-in, loop-out method, leaving the surrounding sequence entirely unaltered [23]. The *sso1Δ sso2* mutants were tested for growth at both 25ºC and 37ºC (**Fig. 4A** and **Fig. S4 A** and **B**). No effect was observed with single, double or triple mutations in the first NPY domain, (*sso1Δ sso2M1-M4)*, however changing all four residues to alanine (*sso1Δ sso2M5*) resulted in reduced growth at 37ºC (**Fig. S4B**). Mutating all four residues of the second NPY domain to alanine (*sso1Δ sso2M6*) did not affect growth at any temperature, however changing all residues of both the first and second NPY domain to alanine (*sso1Δ sso2M7*) resulted in significantly reduced growth at 25ºC and 34ºC and severely impaired growth at 37ºC (**Fig. 4A**). The synergistic effects of eliminating the first and second NPY motif of Sso2 suggest that both motifs are functional and at least partially redundant.

We next assayed the export of two different cell surface enzymes, Bgl2 and invertase. Bgl2 is synthesized and secreted constitutively, while the synthesis of invertase is under hexose repression. Both enzymes become trapped at the cell surface by the cell wall glucan and this external pool can be released by treatment of cells with exogenous glucanase, while any internal pool remains associated with the resulting spheroplasts [24]. Using western blot analysis to measure the internal and external pools of Bgl2, we found that the secretory efficiency at 37ºC generally paralleled growth: *sso1Δ sso2M1-M6* showed only a modest accumulation of an internal pool, while *sso1Δ sso2M7* accumulated a significantly larger internal pool (**Fig. 4 B** and **C** and **Fig. S4 C** and **D**).

To assay invertase secretion we started with cells grown at 25ºC in 5% (w/v) glucose to repress synthesis and then shifted to 0.1% (w/v) glucose to derepress synthesis and simultaneously shifted the cells to 37ºC. Using these conditions we found that *sso1Δ sso2M1-M4* and *sso1Δ sso2M6* were not significantly different from the *sso1 Δ SSO2* control, while *sso1Δ sso2M5* showed a minor defect in invertase secretion and *sso1Δ sso2M7* showed a more substantial defect (**Fig. 4D** and **Fig. S4E**).

Mutation of the Sso2 NPY motifs cause polarized accumulation of secretory vesicles

Defects on the secretory pathway are typically associated with the accumulation of membrane bound intermediates [25]. Loss of function of exocytic SNAREs, including Sso1 and Sso2 leads to the accumulation of secretory vesicles [26]. Secretory vesicles are normally delivered to sites of polarized cell surface growth, such as the tip of the bud, early in the cell cycle and the neck separating the mother cell and bud, late in the cell cycle. Thin section electron microscopy revealed an accumulation of vesicles in the mutants that mirrored their growth: the *sso1Δ SSO2* control and the *sso1Δ sso2M6* mutant had relatively few vesicles per cell section, while *sso1Δ sso2M5* and *sso1Δ sso2M7* had many more (**Fig. 5 A-E**). The vesicles were similar in size in the different strains (**Fig. 5F**) and were found preferentially within the buds of small budded cells (**Fig. 5 A-D**).

Mutations in the NPY motifs of Sso2 affect Snc1 recycling

In addition to the export of newly synthesized cell surface proteins, secretory vesicles are also important for recycling certain plasma membrane proteins back to the cell surface after they have been internalized by endocytosis. The Snc1 v-SNARE has been shown to rapidly cycle from secretory vesicles to the plasma membrane, and then into endocytic vesicles from which it is recycled through the Golgi into a new round of secretory vesicles [27]. Under normal growth conditions, Snc1 is predominantly found on the plasma membrane, with only a minor pool in internal structures. Impeding any step in the cycle leads to a shift in the steady state distribution of GFP-Snc1. We examined the distribution of GFP-Snc1 in various *sso1Δ sso2* mutants. In the *sso1Δ SSO2* control and the *sso1Δ sso2M6* mutant, GFP-Snc1 was mostly on the plasma membrane with a small number of internal, patch-like structures apparent (**Fig. 6 A** and **C**). In contrast, the *sso1Δ sso2M5* and *sso1Δ sso2M7* mutants showed a much greater fraction of cells with internal patches of GFP-Snc1, presumably representing concentrations of secretory vesicles, and a greatly reduced localization to the plasma membrane (**Fig. 6 B, D** and **E**).

The *sso2* mutations have no effect on the actin-independent localization of Sec3

Secretory vesicles are delivered to sites of cell surface growth by the type V myosin, Myo2, moving along polarized actin cables [28]. Loss of actin or Myo2 function leads to the rapid depolarization of a vesicle marker, such as the Rab GTPase Sec4 [29]. Sec3, in contrast remains associated with the tips of small buds and the necks of large buds even after actin polymerization has been blocked by addition of Latrunculin A (LatA) [30]. We determined if the interactions between Sec3 and the NPY motifs of Sso2 are required for the actin-independent localization of Sec3. GFP-Sec4 and Sec3-3×GFP were

expressed in *sso1Δ SSO2, sso1Δ sso2M5* and *sso1Δ sso2M7* cells. Localization was evaluated after treatment with either LatA or DMSO for 15 min. The polarized localization of GFP-Sec4 was lost after treatment with LatA (**Fig. 7 A** and **B**). While the localization of Sec3-3×GFP was largely resistant to LatA treatment in the control and *sso1Δ sso2M5* mutant cells, the polarization of Sec3-3×GFP in *sso1Δ sso2M7* was only slightly reduced by LatA treatment (**Fig. 7 C** and **D**). These results demonstrate that the NPY motifs of Sso2 do not play a major role in the recruitment of Sec3 to sites of polarized growth. Prior studies have shown that the actin-independent localization of Sec3 involves its interaction with the Rho1 and Cdc42 GTPases [31, 32].

Discussion

Sec3 is a subunit of the octameric exocyst complex, a tethering factor that marks the docking site for secretory vesicles in exocytosis. Sec3 is recruited to these sites by binding to the membrane-anchored small GTPases Rho1/Cdc42 and phosphoinositides on the plasma membrane [31-34]. Sso2, similar to its homologous t-SNARE in neuronal exocytosis, bears a C-terminal transmembrane helix. We have previously reported crystal structures of the Sec3 N-terminal PH domain in complex with the closed form of Sso2 as a four-helix bundle [22]. We found that Sec3 destabilizes the linker between Hc and H3 of Sso2 via an allosteric effect, which promotes the assembly of the binary complex between Sso2 and the other t-SNARE, Sec9, and thus drastically accelerates subsequent full SNARE assembly with the v-SNARE Snc1/2 to drive fusion of secretory vesicles with the plasma membrane. However, it remains unknown whether the conserved N-terminal

extension of Sso2 also participates in the Sso2/Sec3 interaction and how Sso2 is effectively recruited to Sec3.

Here we report a new crystal structure of the Sec3 PH domain in complex with a nearly full-length version of Sso2 that contains all sequence except for the C-terminal transmembrane helix. In addition to the interaction between the helical bundle of Sso2 and Sec3 observed in the previous study, we found an extra interaction interface between two conserved NPY motifs at the N-terminal end of Sso2 and a hydrophobic pocket on Sec3 (**Fig. 1B**). The NPY motifs are connected to the highly conserved helical core of Sso2 via a non-conserved linker with variable lengths (roughly 15-40 residues), which is invisible in our crystal structure, suggesting that it is mobile within the crystal structure.

There are two copies of the Sso2/Sec3 complex in our crystal structure. The two NPY motifs were independently bound to Sec3 in these two complex structures (**Fig. 2**). Despite variations in the flanking residues, the cores of the two motifs, i.e. residues Asn, Tyr and Pro, adopt essentially the same conformation and have similar hydrogen bond networks with the neighboring Sec3 residues and water molecules (**Fig. S3**). Our ITC experiments show that although either of the two NPY motifs alone could bind Sec3, their binding affinities were 3-4 fold lower than the polypeptide with both motifs (**Fig. 3**). Similarly, mutation of either motif to alanine also substantially reduced the interaction of the N-terminal part of Sso2 with Sec3, whereas simultaneous mutation of both motifs completely abolished the interaction. Together these data suggest that the two NPY motifs bind Sec3 synergistically.

To further understand the function of the NPY motifs in exocytosis, we carried out a series of *in vivo* assays using strains carrying mutations of Sso2 in its NPY motifs. While

mutation of either NPY motif only slightly reduced cell growth, simultaneous mutation of both NPY motifs severely impaired cell growth, particularly at 37ºC (**Fig. 4A**). We also explored how mutations of the NPY motifs of Sso2 influence protein secretion using Bgl2 and invertase as reporters. Our data show that mutation of both motifs simultaneously substantially affects cell secretion efficiency, with a significantly larger internal pool of Bgl2 failing to reach the cell surface, whereas mutation of either motif alone yielded only a modest accumulation of an internal pool (**Fig. 4 B** and **C** and **Fig. S4 C** and **D**). Similar effects were observed in invertase secretion, where the double NPY mutant showed a more substantial defect than all other mutants (**Fig. 4D** and **Fig. S4E**).

We further checked how the *sso*2 NPY mutations affect fusion of secretory vesicles to the target sites on the plasma membrane. Mutation of both NPY motifs resulted in the accumulation of many vesicles within the cell. Similar results were also observed for the mutation of the first NPY motif, whereas that of the second NPY motif showed no significant effect (**Fig. 5**). Consistently, we found that both the double NPY mutation and mutation of the first NPY motif caused accumulation of GFP-Snc1 patches within the cytoplasm (**Fig. 6**). Taken together, we conclude that the NPY motifs of Sso2 play an essential role in the secretory pathway. Notably, however, the interaction between Sec3 and the NPY motifs of Sso2 is dispensable for the actin-independent localization of Sec3 (**Fig. 7**), which is consistent with previous reports that recruitment of Sec3 to the plasma membrane is determined by its interaction with the small GTPases Rho1 and Cdc42 as well as phosphoinositides on the membrane [31-34].

In the structure with the second NPY motif bound to Sec3 we see extra electron densities beyond the bound NPY motif. However, the quality of the map in that part was

poor and we could only build the main chains for residues 6-9 (**Fig. 8A**). We found that this “fuzzy” part upstream of the bound NPY motif is in close contact with the C-terminal tip of the SNARE motif (i.e. H3) of Sso2 (**Fig. 8B**). Given that binding of Sec3 destabilizes the linker connecting H3 to Hc and prepares H3 for its subsequent interaction with Sec9, a possible role for the NPY motif might be to serve as a stopper to hold the destabilized SNARE motif in place to prevent a premature release of H3 before it is ready to form a binary complex with the other t-SNARE protein Sec9.

The dual interaction interfaces between Sso2 and Sec3 are reminiscent of what have been seen in the structures of syntaxin-1 and Tlg2 in complex with their partner SM proteins Munc18 and Vps45, respectively (**Fig. 8 C-E**). In the latter two complex structures, a short peptide at the N terminus of Munc-18 and Vps45, which was named the “N-peptide”, forms a short helix and binds distally to the backside of the first domain of Munc18 or Vps45, opposite to their interaction sites with the helical bundles of the SNARE proteins [35, 36]. In contrast, the binding site for the NPY motifs of Sso2 is on the same side of the Sec3 PH domain as the aforementioned direct contact with the C-terminal part of H3 of Sso2 (**Fig. 8F**). Furthermore, the Sec3 PH domain is a single globular domain and much smaller than Munc18 and Vps45, both of which contain three domains that are folded into a horseshoe-like conformation. The helical bundle of syntaxin-1 and Tlg2 is clamped between the two tips of the “horseshoe”. Additionally, in those two complex structures, the C-terminal extensions of the SNARE motifs (i.e. H3) form a short helix and insert into a hydrophobic pocket deeply inside the “horseshoe” (**Fig. 8 D** and **E**). These together ensure a strong interaction between the two t-SNAREs and their partner SM proteins. In contrast, the interaction interface between Sec3 and Sso2 is

very small. Therefore the interaction between Sec3 and Sso2 is presumably much weaker than that in the Munc18/syntaxin-1 and Vps45/Tlg2 complexes. Our ITC data show that double mutation of both NPY motifs completely abolished the interaction between the N terminal part of Sso2 and Sec3. Consistently, our *in vivo* data demonstrate that simultaneous mutation of both NPY motifs substantially impaired protein secretion as well as recycling of cell surface proteins. We therefore think that another important role for the NPY motifs is to enhance the interaction of Sso2 with Sec3 by providing an additional binding site to ensure effective recruitment of Sso2 to vesicle docking sites on the plasmas membrane.

Notably, the N-peptide motif is ubiquitously present in all syntaxins that interact with SM proteins [37-40]. It serves as an initiator to recruit SM proteins to their SNARE partners to facilitate their subsequent assembly [41]. Given that the NPY motifs are linked to the rest of Sso2 via a long variable linker, we hypothesize that they may similarly function like fishing hooks to search for Sec3 around the membrane-anchored Sso2 (**Fig. S5**). Once the “hooks” find and bind to Sec3, Sso2 would be locally restrained, which would promote the binding of Sec3 to the helical bundle of Sso2. This would in turn lead to the destabilization of the linker between Hc and H3 of Sso2 and thus promote the assembly of the binary complex between Sso2 and Sec9 to facilitate the final formation of the full SNARE complex with the v-SNARE Snc1/2, which drives the fusion of secretory vesicles with the plasma membrane.

Materials and Methods

Molecular cloning of expression constructs for *in vitro* assays

The Sso2 sequence excluding only its C-terminal transmembrane domain (aa1-270) and the Sec3 PH domain sequence (aa75-260) were both sub-cloned into the pET-15b vector (Novagen) between the *Nde*I and *BamH*I sites. This plasmid provides an N-terminal His_6 tag followed by a thrombin cleavage site prior to the target proteins. All constructs were validated by DNA sequencing.

Protein expression and purification

The *E. coli* strain BL21(DE3) cells harboring the expression plasmids for Sso2 and Sec3 were cultured in Luria Broth (LB) medium containing 50 mM ampicillin at 37°C to an OD_{600} of 0.6-0.8. Over-expression of the target proteins was induced using 0.5 mM isopropylthio-β-d-galactoside (IPTG) and cultures were incubated at 18°C overnight. Cells were harvested by centrifugation (6,000×g, 12 min, 4°C). The pellets were resuspended in pre-chilled lysis buffer containing 20 mM HEPES (pH 7.5), 100 mM NaCl, 20 mM imidazole, and 10 mM beta-mercaptoethanol. Cell were lysed using an EmulsiFlex-C3 homogenizer (Avestin). After centrifugation (25,000×g, 40 min, 4°C) to remove cell debris the supernatant was filtered through a 0.45-μm pore size filter and then loaded onto a 5-ml Ni-HiTrap column (GE Healthcare) that had been pre-equilibrated in the same lysis buffer. After washing with 5 column volumes (cv) of lysis buffer, bound protein was eluted using a linear gradient concentration of imidazole in the lysis buffer (20 to 600 mM, 25×cv). Elution fractions were checked on SDS-PAGE gels and those containing target proteins were pooled. The N-terminal His_6 tag was removed by incubating the purified proteins with ~3% (w/w) thrombin (4°C, overnight) and then subjected to SEC using a Superdex S-200 16/60 column (GE Healthcare) pre-equilibrated

with the running buffer containing 20 mM HEPES (pH 7.5), 100 mM NaCl, and 1mM DTT. Fractions of interest were pooled for later use.

To generate protein complex for crystallization, purified domains of Sec3 and Sso2 were mixed in a molar ratio of 2:1. After incubation at 4°C for one hour, the mixture was loaded on a Superdex S-200 16/60 column (GE Healthcare) pre-equilibrated with the same running buffer as above. Elution fractions were checked on a 15% (w/v) SDS-PAGE gel. The first elution peak containing both proteins were pooled and concentrated to 10-15 mg/ml using Amicon Ultra Centrifugal Filter Units (Millipore) with 10-kDa molecular weight cutoffs.

Crystallization, data collection, and structure determination

Concentrated protein of the Sec3-Sso2 complex (~12 mg/ml) was subjected to extensive crystallization screening trials using commercial crystallization kits. Initial crystallization screenings were carried out at 22ºC by the sitting drop vapor diffusion method using the Phoenix HT liquid handling robot (Rigaku) to set up dual droplets for each condition with drop volume of 0.2 and 0.3 µl (1:1 and 2:1, protein vs reservoir solution) on 96-well sitting drop crystallization plates (Molecular Dimensions). The crystal used for final data collection was grown from a manually set up droplet containing 2 µl of protein and 1 µl of reservoir solution. Needle-shaped crystals of ~10 × 10 × 100 µm were obtained in a condition containing 0.1 M sodium acetate (pH 5.0), 0.2 M ammonium acetate, and 30% (w/v) PEG 4,000. All crystals were harvested with nylon loops (Hampton Research) by flash-cooling in liquid nitrogen using the same reservoir solutions containing 20% (v/v) glycerol as cryo-protectant. X-ray diffraction data were collected at

the beamline ID23-1 of the European Synchrotron Radiation Facility (ESRF) in Grenoble, France. Data reduction was carried out using the XDS program [42].

For structure determination, the maximum-likelihood molecular replacement by PHASER [43] was conducted using our previously determined structures of Sec3 and Sso2 (PDB code: 5M4Y) as the searching model [22]. The structural models were carefully checked; all different regions as well as extra parts in the models where electron densities were clearly visible were manually built using the program COOT [44]. Refinement was carried out by Phenix.refine [45] using data of 20-2.19 Å. All subsequent structure analyses and figure generations were carried out using Pymol (http://www.pymol.org). The details of data collection and refinement statistics are summarized in Supplementary Table 1.

Isothermal titration calorimetry (ITC)

ITC measurements were conducted on a MicroCal PEAQ-ITC microcalorimeter (Malvern Panalytical). Purified Sec3 (aa75-260) protein was dialyzed overnight against a buffer composed of 20 mM HEPES (pH 7.5), 100 mM NaCl, and 1 mM DTT. Synthetic Sso2 polypeptides were dissolved in the same buffer and their concentrations were determined using the DS-11+ Spectrophotometer (DeNovix). For each ITC measurement the cell held 250 µl of 59 µM Sec3, while the injection syringe contained 45 µl of the 590 µM respective titrants. The experiments consisted of one initial 0.4 µl injection followed by 18 consecutive 2 µl injections with a duration of 4 sec each at an interval of 120 sec. The resulting data were analyzed using the MicroCal PEAQ-ITC Analysis Software (Malvern Panalytical, Version 1.22) using the one-set-of-site fitting model. Non-linear least square

fitting using one binding site model was used to calculate the association constant (K_a). Dissociation constants (K_d) were calculated according to the formula $K_d = 1/K_a$.

Construction of strains and plasmids for *in vivo* assays

To generate the various *sso2* mutants, a fragment of the *SSO*2 gene consisting of the promotor region (242bp) and a C-terminally truncated ORF (1-659 bp) was amplified by PCR. The PCR product was digested and ligated into *Kpn*I/*Hind*III enzyme sites in an integrative pRS306 based vector. The *sso2* mutations were generated by QuikChange Lightning Site-Directed Mutagenesis Kit (Aligent, #210518).

Plasmids carrying the mutant alleles were linearized by digestion with the *Msc*I enzyme to promote integration into the *SSO2* locus and introduced into yeast strains (an *sso1Δ* strain for mutants *sso2M1-M6* or wt for *sso2M7*) by the lithium acetate method. Transformants were selected on SC-Ura plates. Multiple independent transformants were grown in SC-Ura medium overnight. To select for Ura- "loop-out" segregants, cells (100 µl) were collected, washed in sterile water, and then plated on YPD+5-FOA plates. Integration and loop-out events leading to the genomic expression of the *sso2* mutations were verified by sequencing PCR products. Due to genetic instability issues, we used a two-step procedure to construct an *sso1Δ sso2M7* strain. A wt strain was transformed with plasmid NRB1659 and then Ura- cells were selected by growth on 5-FOA plates. The selected *sso2M7* strain was crossed with an *sso1ΔSSO2* strain and, after dissection haploid *sso1Δ sso2M7* spores were identified by PCR analysis.

Growth test

Mutants were grown in yeast extract peptone dextrose (YPD) medium overnight to stationary phase. 0.04 OD_{600} units of cells were resuspended in 200 ul sterile water and diluted in fivefold serial dilutions. Cells were spotted on YPD plates and incubated at 25ºC, 34ºC, or 37ºC for 2 days.

Bgl2 secretion assay

The Bgl2 secretion assay was carried out as previously described by Yuan et al [24]. Briefly, 15 mL of yeast cells were grown at 25°C in YPD medium overnight to early log phase (~0.5 OD_{600}/mL), then shifted to 37°C for 90 min. 6 OD_{600} units of cells from each strain were harvested by centrifugation at 900 × *g* for 5 min. Cell pellets were resuspended in 1 mL of ice-cold 10 mM NaN_3 and 10 mM NaF, and then incubated on ice for 10 min. The cell suspension was transferred to 1.5 ml microfuge tubes, pelleted, and resuspended in 1 mL of fresh prespheroplasting buffer consisted of 100 mM Tris-HCl (pH 9.4), 50 mM β-mercaptoethanol, 10 mM NaN_3, and 10 mM NaF, then incubated on ice for 15 min. Cells were then pelleted and washed with 0.5 mL of spheroplast buffer (50 mM KH_2PO_4-KOH (pH 7.0), 1.4 M sorbitol, and 10 mM NaN_3). Cells were resuspended in 1 mL of spheroplast buffer containing 167 µg/mL zymolyase 100T (Nacasai Tesque) and incubated at 37°C in a water bath for 30 min. Spheroplasts were spun down at 5,000 × *g* for 10 min, and 100 µL of the supernatant from each tube was transferred into a new 1.5-ml tube and mixed immediately with 34 µL of 4× SDS sample buffer (the external pool). All of the remaining supernatant was discarded. The pellets (spheroplasts) were

resuspended in 100 µL 1×SDS sample buffer (the internal pool). Samples were boiled for 10min and proteins were separated on a 10% SDS/PAGE gel. Bgl2 was visualized by Western blotting with anti-Bgl2 rabbit polyclonal antibody at 1:5,000 dilution (provided by the laboratory of Randy Schekman, University of California, Berkeley). For quantitation of Bgl2, images of western blots were captured using the ChemiDoc system (Bio Rad) and multiple images were collected to ensure an unsaturated signal. Serial dilutions of a control sample were run in parallel to establish a standard curve. The electrophoretic bands were quantitated using ImageJ software (https://imagej.nih.gov).

Invertase Secretion Assay

The invertase assays were performed as previously described by Yuan et al [24]. Yeast strains were grown at 25°C in YP medium containing 5% (w/v) glucose overnight to early log phase (~0.5 OD_{600}/ml). Then, 1OD_{600} unit of cells was transferred to 2 sets of 15 ml centrifuge tubes and pelleted at 3500 rpm for 5 min. The first set of cells were washed in 0.5 ml sterile water and resuspended in 1 ml ice cold 10 mM NaN3, then kept on ice as 0 min samples. The second set of cells were washed once in sterile water and resuspended in 1 ml YP + 0.1% glucose medium, then incubated at 37°C in a water bath with shaking for 45 min. Cells were pelleted and resuspended in 1 ml 10mM NaN3 as 45 min samples. 0.5 ml cells from each 0 min or 45 min samples were used to measure the external invertase. Another 0.5 ml cells of 0 min or 45 min samples were resuspended in spheroblast buffer containing 50 µg/ml zymolyase and incubated at 37°C in a water bath for 45 min to generate spheroplasts. All internal samples were lysed with 0.5 ml 0.5% Triton X-100. A 20 ul aliquot from each internal and external sample was used for

measuring invertase. The percentage of invertase accumulation was calculated by the formula of $(Int_{45m}-Int_{0m})/[(Ext_{45m}-Ext_{0m}) + (Int_{45m}-Int_{0m})]$.

Electron Microscopy

Control (*sso1Δ/SSO2*) or *sso2* mutant cells were grown at 25°C in YPD to an OD_{600} of ~0.5 and then processed for EM study as previously described [24]. In brief, ~10 OD_{600} units of cells were collected using a 0.22-µm filter apparatus, washed with 10 mL of 0.1 M cacodylate (pH 6.8), then resuspended in 10 mL of fixative (0.1 M cacodylate, 4% glutaraldehyde, pH 6.8). Cells were fixed at room temperature for 1 h and then shifted to 4 °C for 16 h. The next day, cells were washed twice with 50 mM KPi (pH 7.5), and then digested in 2 mL of 50 mM KPi buffer containing 0.25 mg/mL Zymolyase 100T at 37°C for 40 min in a water bath with gentle shaking. Cells were then washed twice with ice-cold 0.1 M cacodylate buffer and resuspended in 1.5 mL of cold 2% (w/v) OsO_4 in 0.1 M cacodylate buffer. Cells were incubated for 1 h on ice, washed three times with water, and then incubated in 1.5 mL of 2% (w/v) uranyl acetate at room temperature for 1 h. Cells were dehydrated by a series of ethanol washes and incubated overnight in Durcupan resin. Cells were embedded in fresh Durcupan resin and baked at 60°C for at least 48 h. Sections were stained with lead citrate and uranyl acetate, and images were acquired using a transmission electron microscope (Tecnai G2 Spirit; FEI) equipped with a CCD camera (UltraScan 4000; Eagle).

Fluorescence Microscopy and Quantitative Localization Analysis

GFP-Snc1 localization: Yeast strains expressing GFP-Snc1 were grown at 25°C to early log phase OD_{600} 0.3–0.6 in SC-Ura medium. 500 µL of cells were harvested and resuspended in growth medium for fluorescence imaging. Cultures were shifted to 37ºC for 90 min, then 500 µl samples were collected for fluorescence imaging. Images were acquired with a 100× oil-immersion objective on a widefield fluorescence microscopy system equipped with a Hamamatsu ORCA-ER camera. For each sample, *z*-stacks with a 200-nm slice distance were generated. Images were analyzed using Volocity software 4.8 (Quorum Technology, Inc). For quantitation studies, three independent transformants from each condition were examined under the same condition and 100-200 cells from each strain were scored. Three separate experiments were used to calculate the SD.

LatA treatment of Sec4-GFP and Sec3-3×GFP: Yeast strains were transformed with an integration vector expressing GFP-Sec4 or Sec3-3×GFP. Cells were grown in YPD to around OD_{600} 0.5, then 1OD_{600} unit cells were collected and resuspended in 50ul SC-Ura medium. 1 µl of 10mM LatA was added to the cell suspension and incubated at 25ºC for 15 min. Cells were fixed with 3.7% (v/v) formaldehyde for 60min and washed twice in 0.5 ml PBS. Cells were imaged on a widefield fluorescence microscope. Quantitation analysis was done as described above. Three separate experiments were used to calculate the SD.

Data availability

Coordinates and structure factors for the Sec3-Sso2 complex have been deposited in the Protein Data Bank with accession code (https://www.rcsb.org/structure/7Q83).

Acknowledgments

We thank the staff at the beamline of ID23-1 at the European Synchrotron Radiation Facility (ESRF) for their help with X-ray diffraction. This work was supported by the grants P28231-B28 and I4960-B from the Austrian Science Fund (FWF) to G.D and GM35370 from the National Institutes of Health to P.N.

Author contributions

GD and PJN conceived the project. MP performed *in vitro* binding assays together with KK. HY carried out all *in vivo* analyses. YZ expressed proteins and grew crystals. GD carried out crystal structure determination and all bioinformatics analyses. GD and PJN wrote the manuscript with help of other authors.

Conflict of interest

The authors declare that they have no conflict of interest.

References

1. Ungermann, C. and D. Kummel, *Structure of membrane tethers and their role in fusion.* Traffic, 2019. **20**(7): p. 479-490.
2. Chia, P.Z. and P.A. Gleeson, *Membrane tethering.* F1000Prime Rep, 2014. **6**: p. 74.
3. Brocker, C., S. Engelbrecht-Vandre, and C. Ungermann, *Multisubunit tethering complexes and their role in membrane fusion.* Curr Biol, 2010. **20**(21): p. R943-52.
4. Yu, I.M. and F.M. Hughson, *Tethering factors as organizers of intracellular vesicular traffic.* Annu Rev Cell Dev Biol, 2010. **26**: p. 137-56.
5. Fernandez, I., et al., *Three-dimensional structure of an evolutionarily conserved N-terminal domain of syntaxin 1A.* Cell, 1998. **94**(6): p. 841-9.
6. Sutton, R.B., et al., *Crystal structure of a SNARE complex involved in synaptic exocytosis at 2.4 A resolution.* Nature, 1998. **395**(6700): p. 347-53.
7. Dulubova, I., et al., *A conformational switch in syntaxin during exocytosis: role of munc18.* EMBO J, 1999. **18**(16): p. 4372-82.
8. Fiebig, K.M., et al., *Folding intermediates of SNARE complex assembly.* Nat Struct Biol, 1999. **6**(2): p. 117-23.
9. Demircioglu, F.E., P. Burkhardt, and D. Fasshauer, *The SM protein Sly1 accelerates assembly of the ER-Golgi SNARE complex.* Proc Natl Acad Sci U S A, 2014. **111**(38): p. 13828-33.
10. Takemoto, K., et al., *Distinct sets of tethering complexes, SNARE complexes, and Rab GTPases mediate membrane fusion at the vacuole in Arabidopsis.* Proc Natl Acad Sci U S A, 2018. **115**(10): p. E2457-E2466.
11. Koike, S. and R. Jahn, *SNAREs define targeting specificity of trafficking vesicles by combinatorial interaction with tethering factors.* Nat Commun, 2019. **10**(1): p. 1608.
12. Cai, H., K. Reinisch, and S. Ferro-Novick, *Coats, tethers, Rabs, and SNAREs work together to mediate the intracellular destination of a transport vesicle.* Dev Cell, 2007. **12**(5): p. 671-82.
13. Wang, S., et al., *Munc18 and Munc13 serve as a functional template to orchestrate neuronal SNARE complex assembly.* Nat Commun, 2019. **10**(1): p. 69.
14. Yu, H., et al., *SNARE zippering requires activation by SNARE-like peptides in Sec1/Munc18 proteins.* Proc Natl Acad Sci U S A, 2018. **115**(36): p. E8421-E8429.
15. Jiao, J., et al., *Munc18-1 catalyzes neuronal SNARE assembly by templating SNARE association.* Elife, 2018. **7**.
16. Xu, Y., L. Su, and J. Rizo, *Binding of Munc18-1 to synaptobrevin and to the SNARE four-helix bundle.* Biochemistry, 2010. **49**(8): p. 1568-76.
17. Andre, T., et al., *The Interaction of Munc18-1 Helix 11 and 12 with the Central Region of the VAMP2 SNARE Motif Is Essential for SNARE Templating and Synaptic Transmission.* eNeuro, 2020. **7**(6).
18. Pleskot, R., et al., *Membrane targeting of the yeast exocyst complex.* Biochim Biophys Acta, 2015. **1848**(7): p. 1481-9.
19. Guo, W., et al., *The exocyst is an effector for Sec4p, targeting secretory vesicles to sites of exocytosis.* EMBO J, 1999. **18**(4): p. 1071-80.
20. Boehm, C. and M.C. Field, *Evolution of late steps in exocytosis: conservation and specialization of the exocyst complex.* Wellcome Open Res, 2019. **4**: p. 112.
21. Lipschutz, J.H. and K.E. Mostov, *Exocytosis: the many masters of the exocyst.* Curr Biol, 2002. **12**(6): p. R212-4.
22. Yue, P., et al., *Sec3 promotes the initial binary t-SNARE complex assembly and membrane fusion.* Nat Commun, 2017. **8**: p. 14236.

23. Novick, P. and D. Botstein, *Phenotypic analysis of temperature-sensitive yeast actin mutants.* Cell, 1985. **40**(2): p. 405-16.
24. Yuan, H., et al., *Rewiring a Rab regulatory network reveals a possible inhibitory role for the vesicle tether, Uso1.* Proc Natl Acad Sci U S A, 2017. **114**(41): p. E8637-E8645.
25. Novick, P., C. Field, and R. Schekman, *Identification of 23 complementation groups required for post-translational events in the yeast secretory pathway.* Cell, 1980. **21**(1): p. 205-15.
26. Aalto, M.K., H. Ronne, and S. Keranen, *Yeast syntaxins Sso1p and Sso2p belong to a family of related membrane proteins that function in vesicular transport.* EMBO J, 1993. **12**(11): p. 4095-104.
27. Lewis, M.J., et al., *Specific retrieval of the exocytic SNARE Snc1p from early yeast endosomes.* Mol Biol Cell, 2000. **11**(1): p. 23-38.
28. Pruyne, D., et al., *Mechanisms of polarized growth and organelle segregation in yeast.* Annu Rev Cell Dev Biol, 2004. **20**: p. 559-91.
29. Salminen, A. and P.J. Novick, *The Sec15 protein responds to the function of the GTP binding protein, Sec4, to control vesicular traffic in yeast.* J Cell Biol, 1989. **109**(3): p. 1023-36.
30. Finger, F.P., T.E. Hughes, and P. Novick, *Sec3p is a spatial landmark for polarized secretion in budding yeast.* Cell, 1998. **92**(4): p. 559-71.
31. Guo, W., F. Tamanoi, and P. Novick, *Spatial regulation of the exocyst complex by Rho1 GTPase.* Nat Cell Biol, 2001. **3**(4): p. 353-60.
32. Zhang, X., et al., *Cdc42 interacts with the exocyst and regulates polarized secretion.* J Biol Chem, 2001. **276**(50): p. 46745-50.
33. Zhang, X., et al., *Membrane association and functional regulation of Sec3 by phospholipids and Cdc42.* J Cell Biol, 2008. **180**(1): p. 145-58.
34. Yamashita, M., et al., *Structural basis for the Rho- and phosphoinositide-dependent localization of the exocyst subunit Sec3.* Nat Struct Mol Biol, 2010. **17**(2): p. 180-6.
35. Eisemann, T.J., et al., *The Sec1/Munc18 protein Vps45 holds the Qa-SNARE Tlg2 in an open conformation.* Elife, 2020. **9**.
36. Burkhardt, P., et al., *Munc18a controls SNARE assembly through its interaction with the syntaxin N-peptide.* EMBO J, 2008. **27**(7): p. 923-33.
37. Latham, C.F., et al., *Molecular dissection of the Munc18c/syntaxin4 interaction: implications for regulation of membrane trafficking.* Traffic, 2006. **7**(10): p. 1408-19.
38. McEwen, J.M. and J.M. Kaplan, *UNC-18 promotes both the anterograde trafficking and synaptic function of syntaxin.* Mol Biol Cell, 2008. **19**(9): p. 3836-46.
39. Johnson, J.R., et al., *Binding of UNC-18 to the N-terminus of syntaxin is essential for neurotransmission in Caenorhabditis elegans.* Biochem J, 2009. **418**(1): p. 73-80.
40. Khvotchev, M., et al., *Dual modes of Munc18-1/SNARE interactions are coupled by functionally critical binding to syntaxin-1 N terminus.* J Neurosci, 2007. **27**(45): p. 12147-55.
41. Rathore, S.S., et al., *Syntaxin N-terminal peptide motif is an initiation factor for the assembly of the SNARE-Sec1/Munc18 membrane fusion complex.* Proc Natl Acad Sci U S A, 2010. **107**(52): p. 22399-406.
42. Kabsch, W., *Xds.* Acta Crystallogr D Biol Crystallogr, 2010. **66**(Pt 2): p. 125-32.
43. McCoy, A.J., et al., *Phaser crystallographic software.* Journal of Applied Crystallography, 2007. **40**(Pt 4): p. 658-674.
44. Emsley, P. and K. Cowtan, *Coot: model-building tools for molecular graphics.* Acta Crystallogr D Biol Crystallogr, 2004. **60**(Pt 12 Pt 1): p. 2126-32.
45. Adams, P.D., et al., *PHENIX: a comprehensive Python-based system for macromolecular structure solution.* Acta Crystallogr D Biol Crystallogr, 2010. **66**(Pt 2): p. 213-21.

Figure legends

Figure 1. Crystal structure of the Sso2/Sec3 complex. (**A**) Schematics of the constructs of Sso2 (aa1–270) and Sec3 (aa75–260) used in our structural studies. (**B**) Superposition of the two Sso2/Sec3 complexes in the asymmetric unit of the crystal structure reported here, together with the one reported previously (light grey, pdb code: 5M4Y). (**C**) Stereo view of the $2F_o - F_c$ electron density map contoured at 1.8 σ level around the binding interface. Maps for Sec3 and Sso2 are colored in cyan and orange, respectively.

Figure 2. Structural analyses of the interaction between the NPYmotifs of Sso2 and Sec3. (**A**) Sequence alignments of Sso2 homologs. Conserved residues are shaded in dark (highly conserved) or light blue (partially conserved). The two NPYmotifs are marked as magenta blocks above the aligned sequences, which are connected to helix Ha via a variable linker. (**B**) Ribbon diagram of the crystal structure of the Sso2-Sec3 complex with first NPYmotif (shown as sticks) of Sso2 bound to Sec3. (**C**) An enlarged view of the NPYmotif in (B) together with the 2Fo-Fc map contoured at 1.5σ. (**D**) Sticks of the NPYmotif on top of an electrostatic surface plot of Sec3. (**E-G**) Crystal structure shows how the second NPYmotif of Sso2 interacts with Sec3. (**H**) Move-out view of the binding site shows the cork-like NPYmotif (magenta) and the complementary cradle-like pocket on Sec3 (light blue). The structure is shown as semitransparent surface together with ribbon diagrams (Sec3) or sticks (Sso2). The top broad part of the “cork” of Sso2 is stabilized by a hydrogen bond between the carboxyl group of the Asn (N) sidechain and the amide proton of Tyr (Y).

Figure 3. ITC measurements of the interaction between Sec3 and variant versions of the NPYmotifs of Sso2. (**A**) Wild-type double NPYmotifs of Sso2 bound Sec3 with a dissociation constant (Kd) of approximately 21µM. (**B** & **C**) Either of the two NPYmotifs alone bound Sec3 much more weakly than the two together, with the Kd values dropped by 3-4 fold. (**D** & **E**) Mutation of either NPYmotif (i.e. M5 and M6) also reduced the binding

affinity of Sso2 to Sec3. (**F**) Double mutation (M7) of both NPYmotifs completely abolished the interaction between Sso2 and Sec3. For M6 in (E), the peptide concentration had to be increased by 6 fold to detect its very weak interaction with Sec3.

Figure 4. Mutations in *sso2* inhibit cell growth and secretion of Bgl2 and invertase. (**A**) *sso2* mutants in an *sso1Δ* background partially inhibit cells growth at 37ºC. Control *sso1Δ SSO2* or *sso1Δ sso2* mutant cells were grown overnight in YPD medium. An aliquot (0.2 OD_{600} units) of cells from each strain was collected, serially diluted by 5 fold and spotted onto YPD plates. Plates were incubated at 25ºC, 34ºC or 37ºC for 2 days. (**B-C**) The *sso1Δ sso2* mutants were grown at 25ºC in YPD medium overnight to early log phase and shifted to 37ºC for 90 min. The internal and external fractions were prepared as described in *Materials and Methods.* (**B**) The internal or external pools of Bgl2 were detected by western blotting. Several mutations in *SSO2* caused inhibition of Bgl2 secretion. (**C**) Quantitation of internal Bgl2 was determined by ImageJ. Results were analyzed based on six independent experiments. Error bar represents SD, n=7. *p< 0.005 , **p< 2e5. (**D**) Strains were grown at 25ºC in YP containing 5% (v/v) glucose medium overnight to early log phase. 1OD_{600} unit of cells was collected from each strain and shifted to YP containing 0.1% (v/v) glucose medium, and incubated at 37ºC for 45min. Four independent experiments were performed. Error bars represent SD, n=4. *p < 0.005.

Figure 5. Thin section EM analysis shows polarized accumulation of secretory vesicles in the *sso2M5 and sso2M7* strains. A control *sso1Δ SSO2* strain and *sso1Δ sso2* mutants were grown in YPD medium at 25ºC to an $OD_{600\ nm}$ of ~0.5, then 10 $OD_{600\ nm}$ units of cells were collected and processed for EM analysis: (**A**) *sso1Δ SSO2*, (**B**) *sso1Δ sso2M5*, (**C**) *sso1Δ sso2M6*, and (**D**) *sso1Δ sso2M7*. Scale Bar, 0.5µm. *sso2M5* and *sso2M7* cells contain more secretory vesicles in the bud compared to *SSO2* and *sso2M6* cells. (**E**) Quantitation of secretory vesicles. The number of vesicles/cell was scored in 46 control cells, 49 *sso2M5cells*, 51 *sso2M6* cells and 45 *sso2M7* cells. (**F**)

Measurement of vesicle size. The measurement was analyzed using ImageJ. 23-91 vesicles were measured.

Figure 6. Snc1 recycling is affected in *sso2* mutants. (**A-D**) Representative images of *sso1Δ* SSO2 control, *sso1Δ sso2M5 sso1Δ sso2M6,* and *sso1Δ sso2M7* mutant cells. Strains harboring a CEN plasmid expressing GFP-Snc1 were grown in SC-Ura medium overnight at 25ºC reaching an OD_{600} around 0.5. Cells were further diluted and shifted to 37ºC for 90 min prior to imaging. GFP-Snc1 localized predominantly to the PM in *SSO2* control cells and *sso2M6* cells yet formed GFP patches (indicated by arrows) near small buds or bud necks in *sso2M5* and *sso2M7* mutant cells. Scale bar, 5um. (**E**) Quantitation of cells with GFP-Snc1 patches. GFP-Snc1 patches near bud tips or necks were scored. Error bar represents SD, n=3. *P < 0.05, **P <0.005.

Figure 7. The *sso2* mutations have little effect on the actin-independent localization of Sec3. (**A**) A control *sso1Δ SSO2* strain or *sso1Δ sso2* mutants expressing Sec4-GFP were grown to early log phase in YPD at 25ºC, then $1OD_{600}$ unit cells was collected and resuspended in 50µl SC medium and incubated with 200µM LatA or DMSO at 25ºC for 15min prior to imaging. Images were captured by fluorescence microscopy. Sec4 is normally localized near the tip of small buds (arrow) and the neck of large buds (arrowhead) in DMSO-treated cells. Sec4 localization was disrupted in LatA-treated cells. Scale bar, 5µm (for all images). (**B**) Quantitation of polarized Sec4-GFP. (**C**) A control *sso1Δ SSO2* strain and the *sso1Δ sso2* mutant strains expressing Sec3-3xGFP were grown and treated with LatA or DMSO under the conditions as described in A. Sec3 localization remains polarized after LatA treatment, either at the tips of small bus (arrow) or the necks of large buds (arrow head). Scale bar, 5µm. (**D**) Quantitation of polarized Sec3-3×GFP. Error bars represent SDs based on three independent experiments in each case.

Figure 8. Interaction of the N-terminus of Sso2 with Sec3 in comparison with that in other syntaxin/SM protein complexes. (**A**) Ribbon diagram of the Sso2/Sec3 complex structure with the 2Fo-Fc map around the NPY motif (residue positions are marked by numbers) shown in dots (1.5 σ). The enlarged view shows the close contact between the N-terminal NPY motif and the C-terminal tip of the H3 helix of Sso2 with their 2Fo-Fc maps shown in magenta and blue, respectively. (**B**) Two orthogonal views of the contact site between the N-terminal extension (magenta) and the C-terminal region (green) of Sso2. Sso2 structure is shown as ribbons and sticks together with a semitransparent surface plot. (**C-E**) Comparison of the structures of the Sso2/Sec3, syntaxin-1/Munc18 and Tlg2/Vps45 complexes, with the N-termini of the t-SANREs indicated. (**F**) Superposition of the three complex structures shown in C, D and E.

Table 1. Data collection and refinement statistics

Wavelength (Å)	0.9793
Resolution range (Å)	19.95 - 2.19 (2.27 - 2.19)
Space group	P 1
Unit cell (*a, b, c*; Å)	50.961, 58.402, 83.286
(*α, β, γ*; °)	104.284, 98.494, 113.198
Total reflections	164,051 (15,510)
Unique reflections	40,853 (3,771)
Multiplicity	4.0 (3.9)
Completeness (%)	96.08 (89.79)
I/σ(I)	6.73 (1.18)
Wilson B-factor	31.15
R-*merge*	0.1641 (1.094)
R-*meas*	0.1894 (1.271)
R-*pim*	0.09332 (0.636)
$CC_{1/2}$	0.99 (0.438)
CC*	0.997 (0.781)
Reflections used in refinement	40,587 (3,771)
Reflections used for R-free	2,008 (181)
R-work	0.1990 (0.2864)
R-free	0.2394 (0.3374)
CC(work)	0.943 (0.699)
CC(free)	0.907 (0.601)
Number of non-hydrogen atoms	5,837
macromolecules	5,419
solvent	418
Protein residues	658
RMS(bonds)	0.002
RMS(angles)	0.50
Ramachandran favored (%)	97.82
Ramachandran allowed (%)	2.18
Ramachandran outliers (%)	0.00
Rotamer outliers (%)	0.00
Clashscore	5.76
Average B-factor	40.87
macromolecules	40.74
solvent	42.65

Statistics for the highest-resolution shell are shown in parentheses.

Figure 1

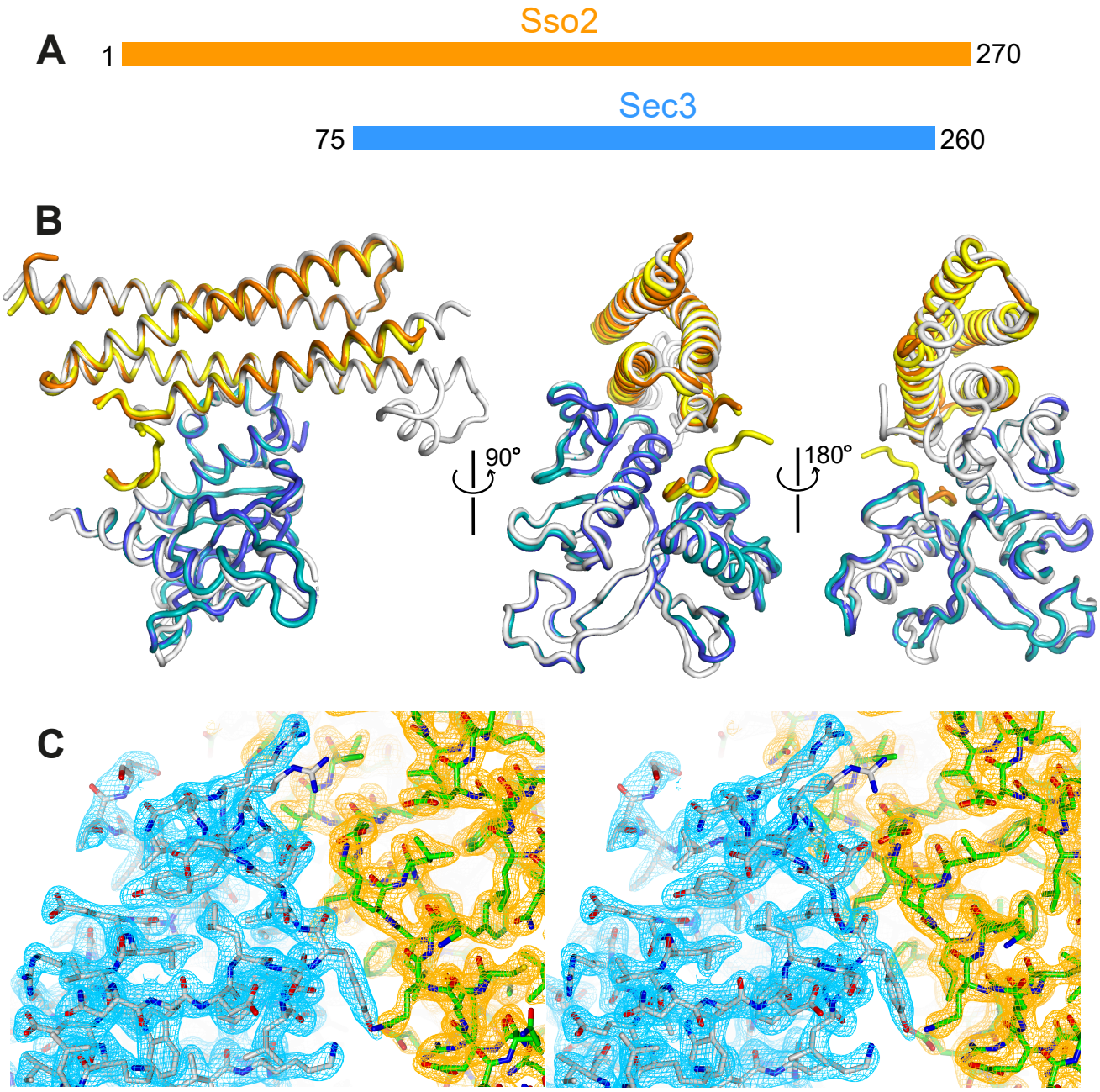

Figure 2

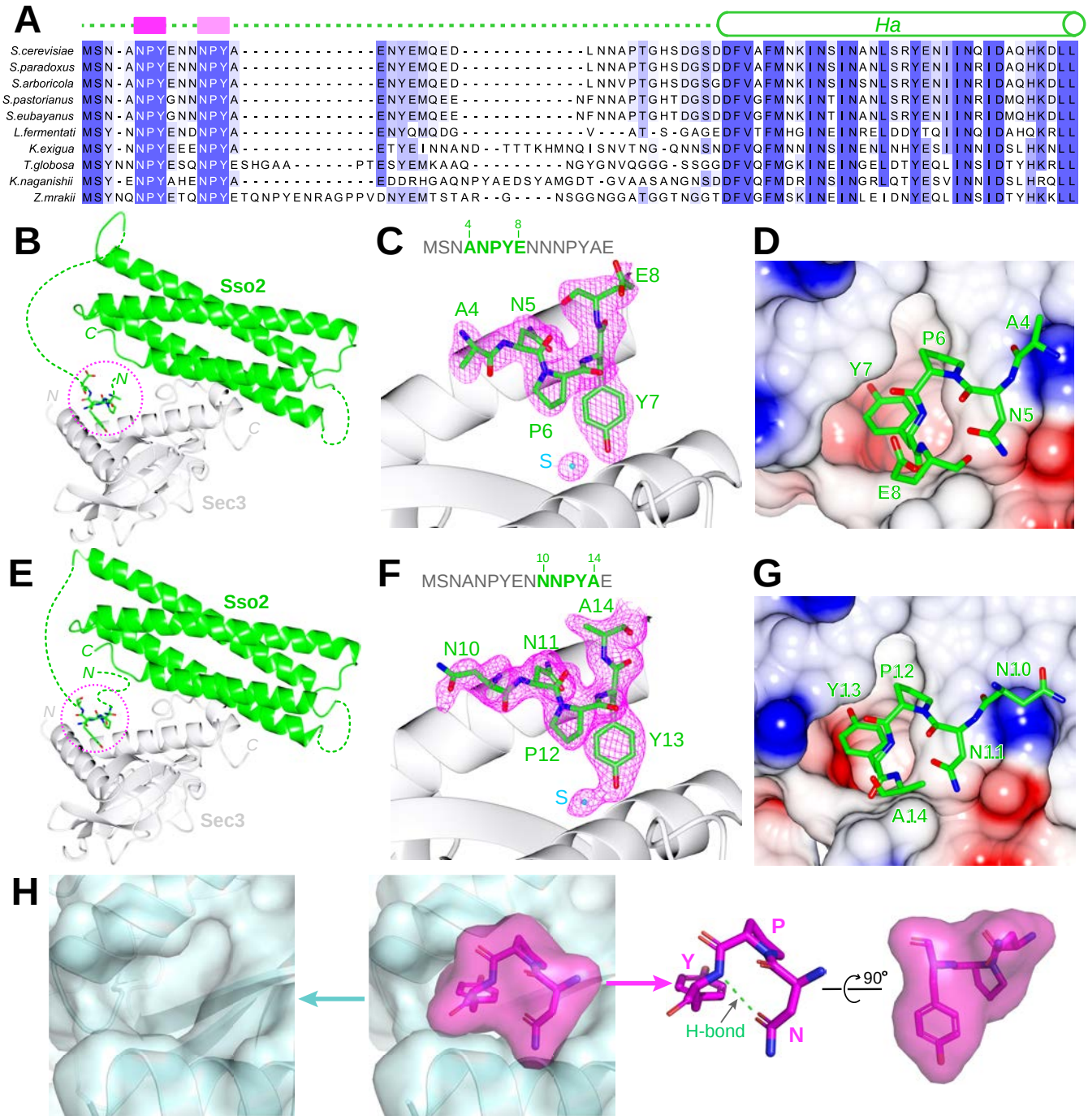
A
Ha
S.cerevisiae
S.paradoxus
S.arboricola
S.pastorianus
S.eubayanus
L.fermentati
K.exigua
T.globosa
K.naganishii
Z.mrakii
B
Sso2
C
N
Sec3
C
MSNANPYENNNPYAE
4
8
A4
N5
E8
Y7
P6
S
D
A4
P6
Y7
N5
E8
E
Sso2
C
N
Sec3
F
MSNANPYENNNPYAE
10
14
A14
N10
N11
Y13
P12
S
G
P12
N10
Y13
N11
A14
H
P
Y
H-bond
N
90°

Figure 3

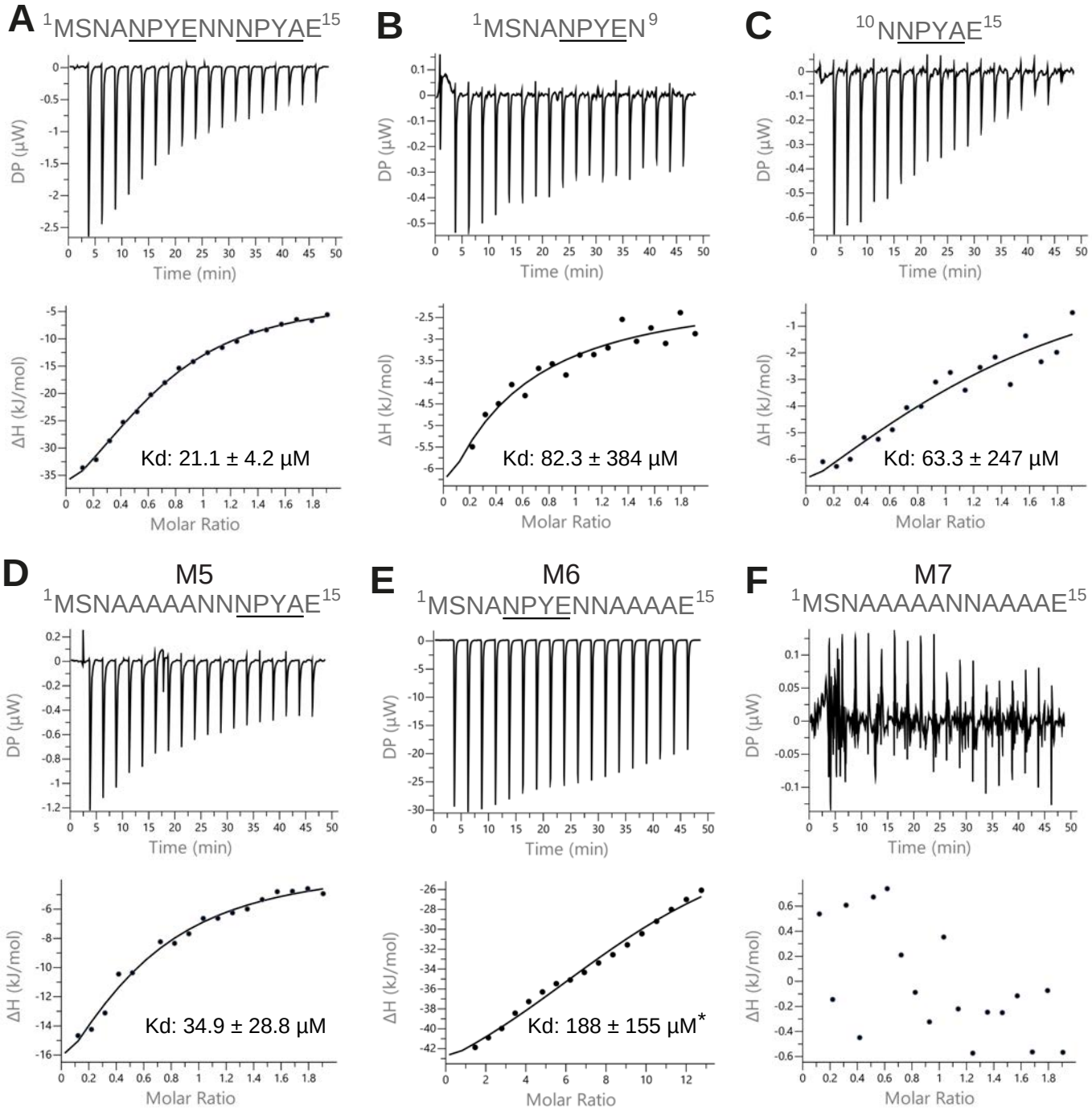
A
1MSNANPYENNNPYAE15
B
1MSNANPYEN9
C
10NNPYAE15
DP (µW)
Time (min)
ΔH (kJ/mol)
Molar Ratio
Kd: 21.1 ± 4.2 µM
Kd: 82.3 ± 384 µM
Kd: 63.3 ± 247 µM
D
M5
1MSNAAAAANNNPYAE15
E
M6
1MSNANPYENNAAAAE15
F
M7
1MSNAAAAANNAAAAE15
Kd: 34.9 ± 28.8 µM
Kd: 188 ± 155 µM*

Figure 4

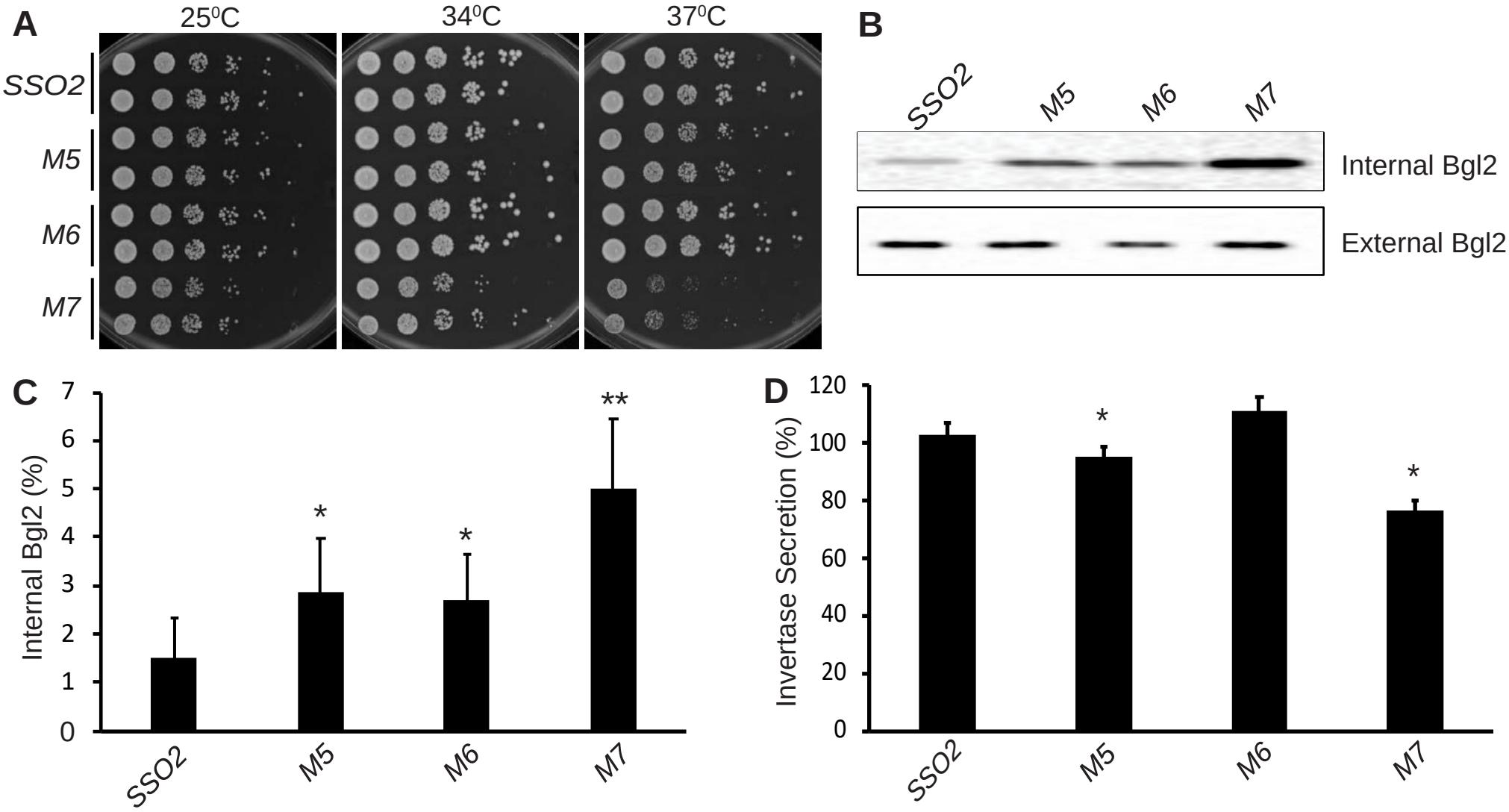
A
25⁰C
34⁰C
37⁰C
SSO2
M5
M6
M7
B
SSO2
M5
M6
M7
Internal Bgl2
External Bgl2
C
Internal Bgl2 (%)
0
1
2
3
4
5
6
7
*
*
**
SSO2
M5
M6
M7
D
Invertase Secretion (%)
0
20
40
60
80
100
120
*
*
SSO2
M5
M6
M7

Figure 5

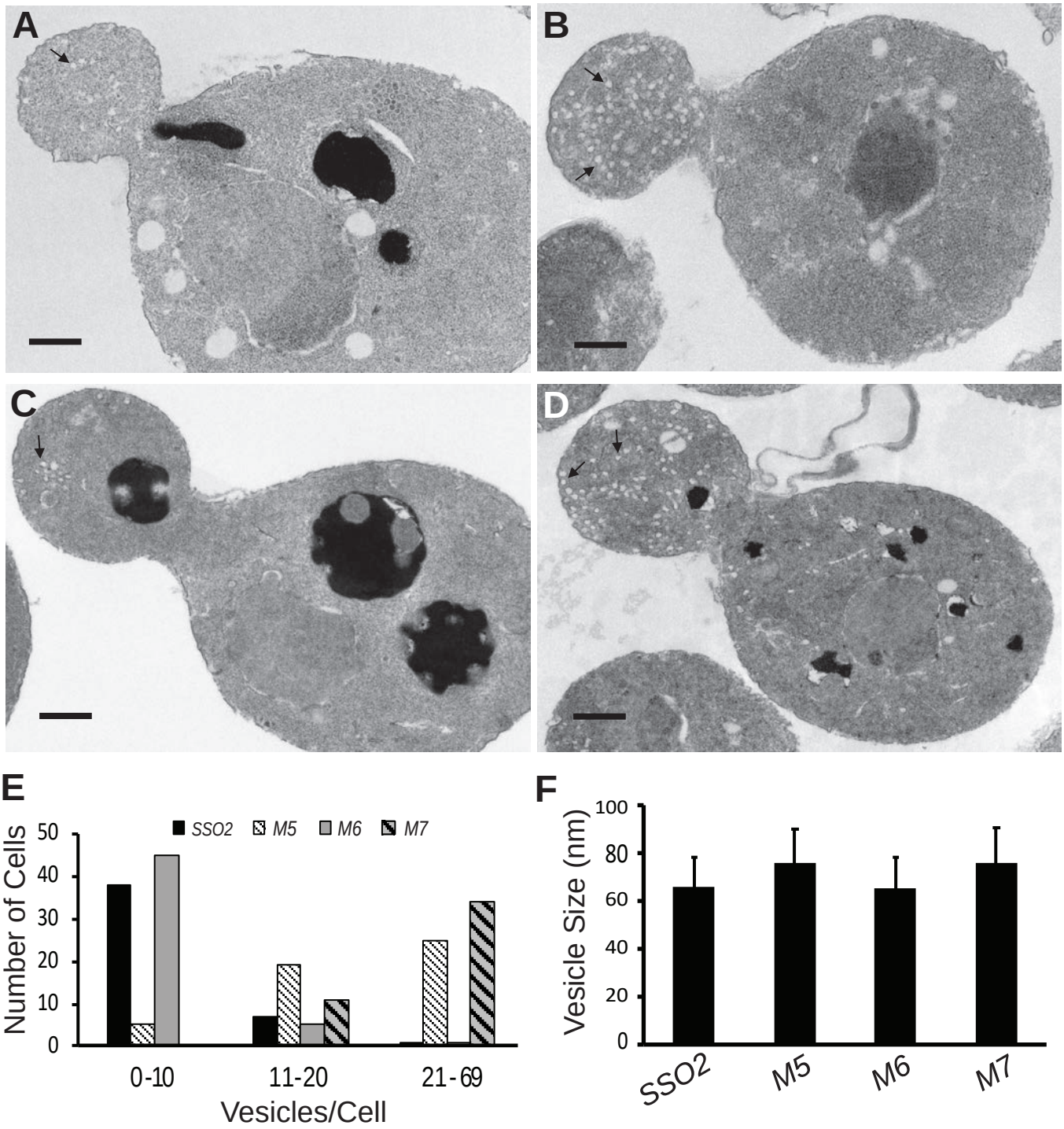
A
B
C
D
E
SSO2
M5
M6
M7
Number of Cells
50
40
30
20
10
0
0-10
11-20
21-69
Vesicles/Cell
F
Vesicle Size (nm)
100
80
60
40
20
0
SSO2
M5
M6
M7

Figure 6

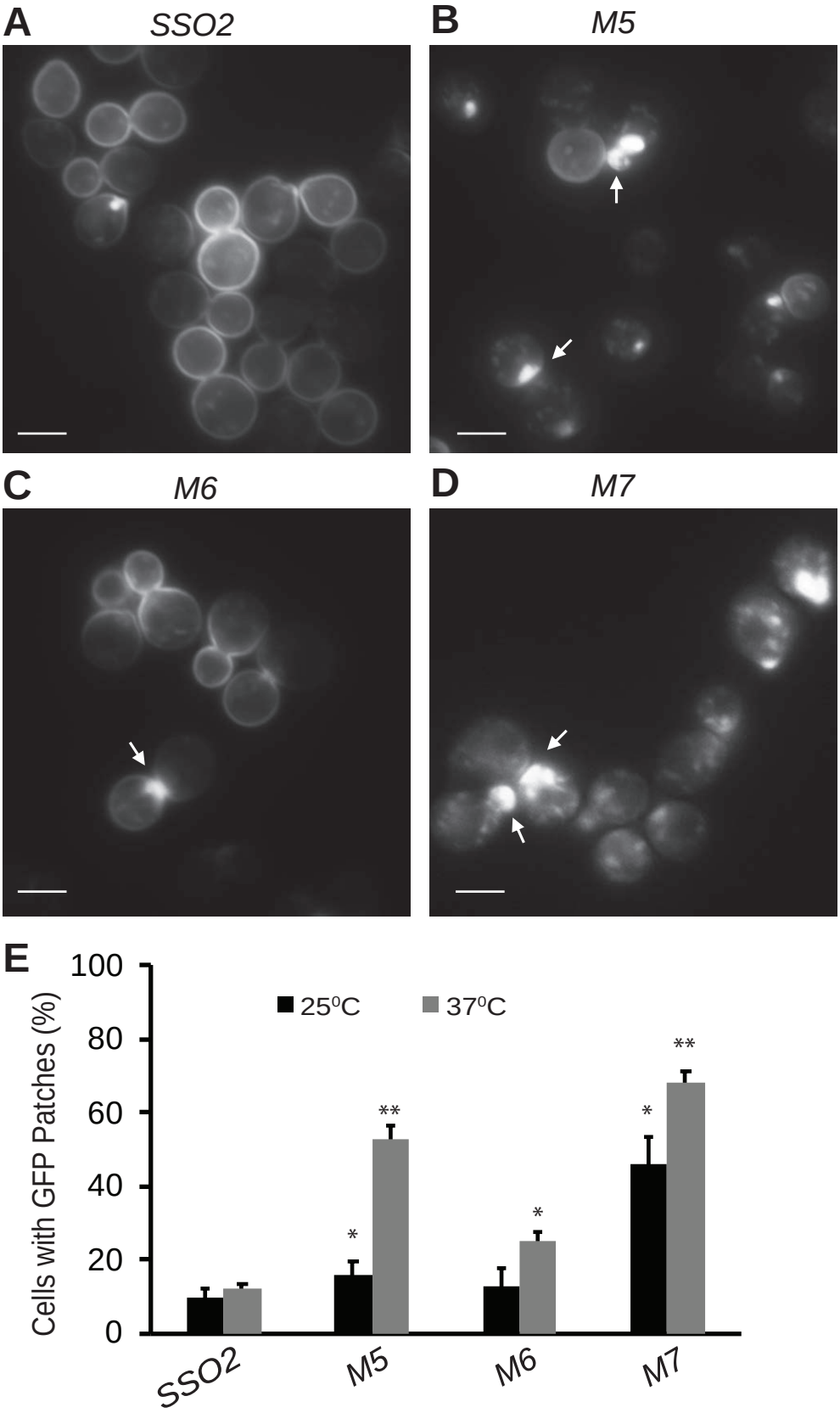
A
SSO2
B
M5
C
M6
D
M7
E
Cells with GFP Patches (%)
100
80
60
40
20
0
25⁰C
37⁰C
*
**
*
*
**
SSO2
M5
M6
M7

Figure 7

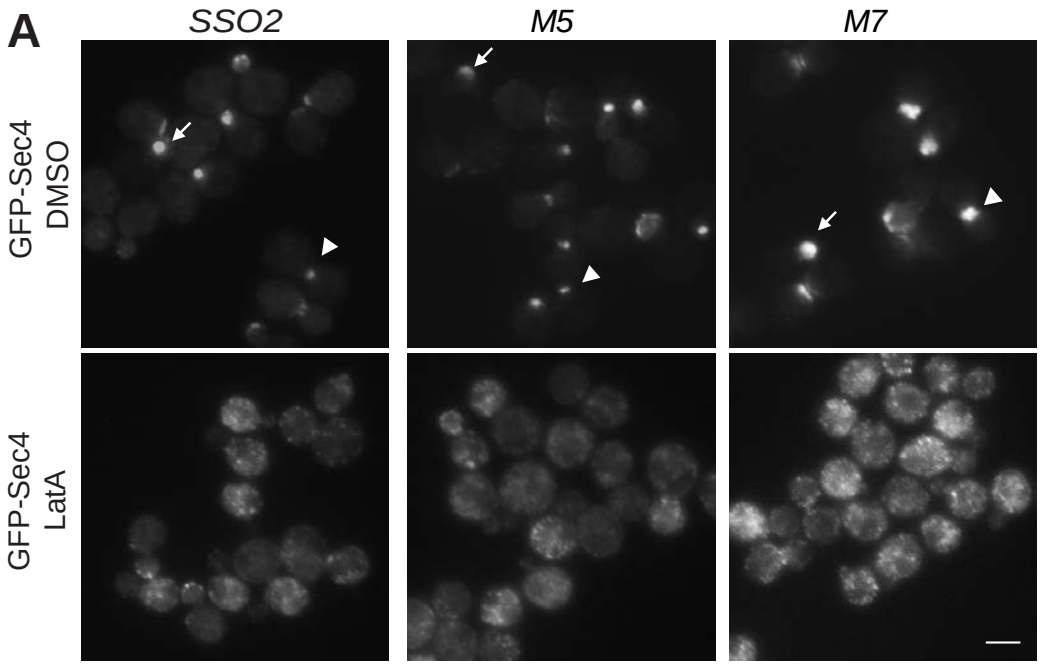
A
SSO2
M5
M7
GFP-Sec4
DMSO
GFP-Sec4
LatA

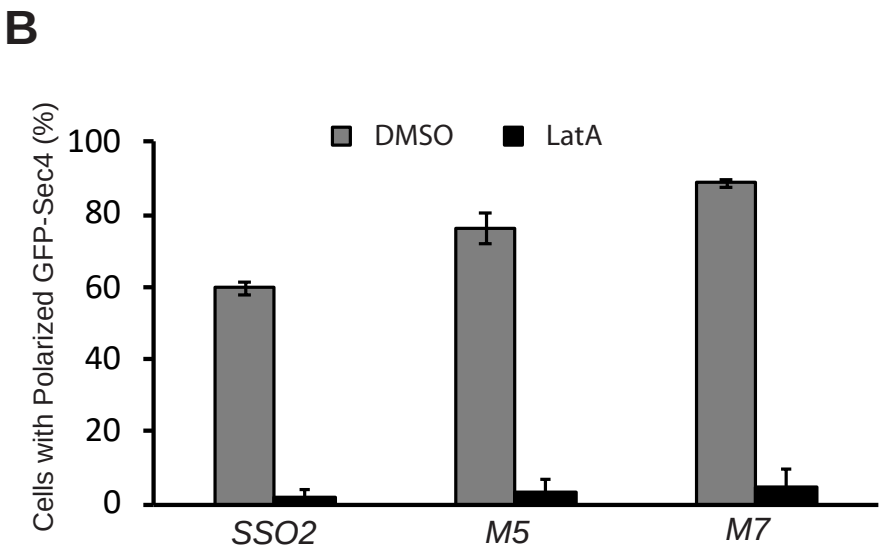
B
DMSO
LatA
Cells with Polarized GFP-Sec4 (%)
100
80
60
40
20
0
SSO2
M5
M7

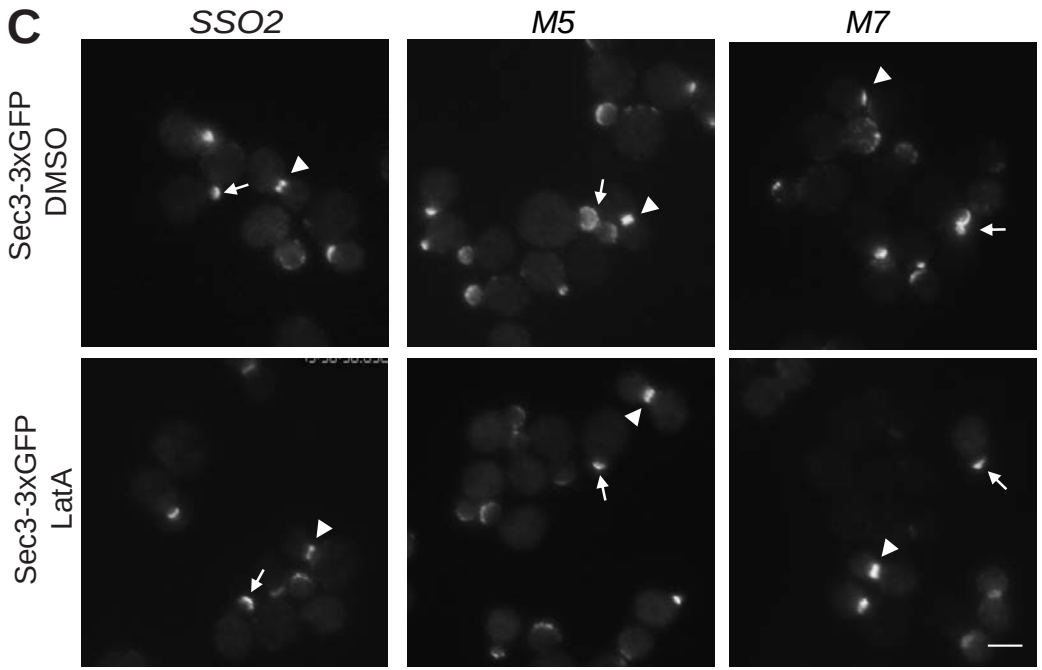
C
SSO2
M5
M7
Sec3-3xGFP
DMSO
Sec3-3xGFP
LatA

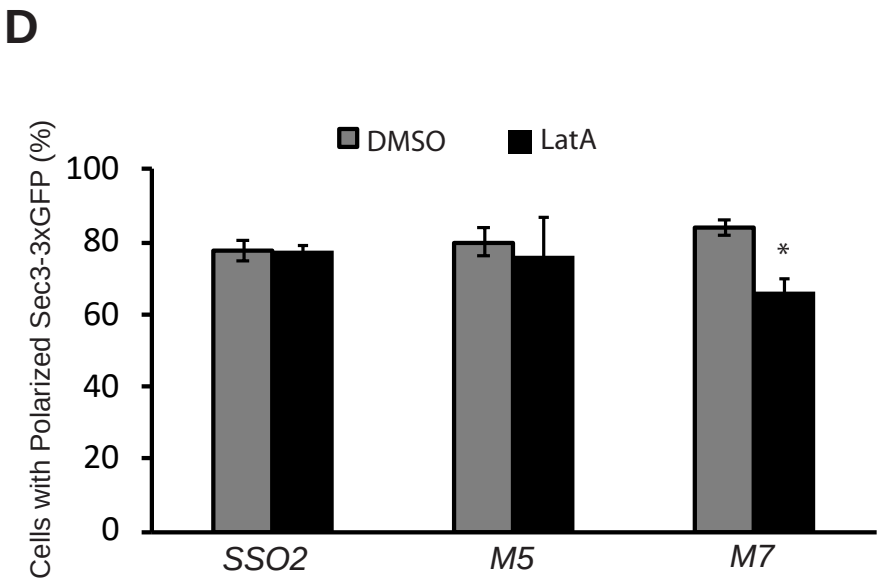
D
DMSO
LatA
Cells with Polarized Sec3-3xGFP (%)
100
80
60
40
20
0
*
SSO2
M5
M7

Figure 8

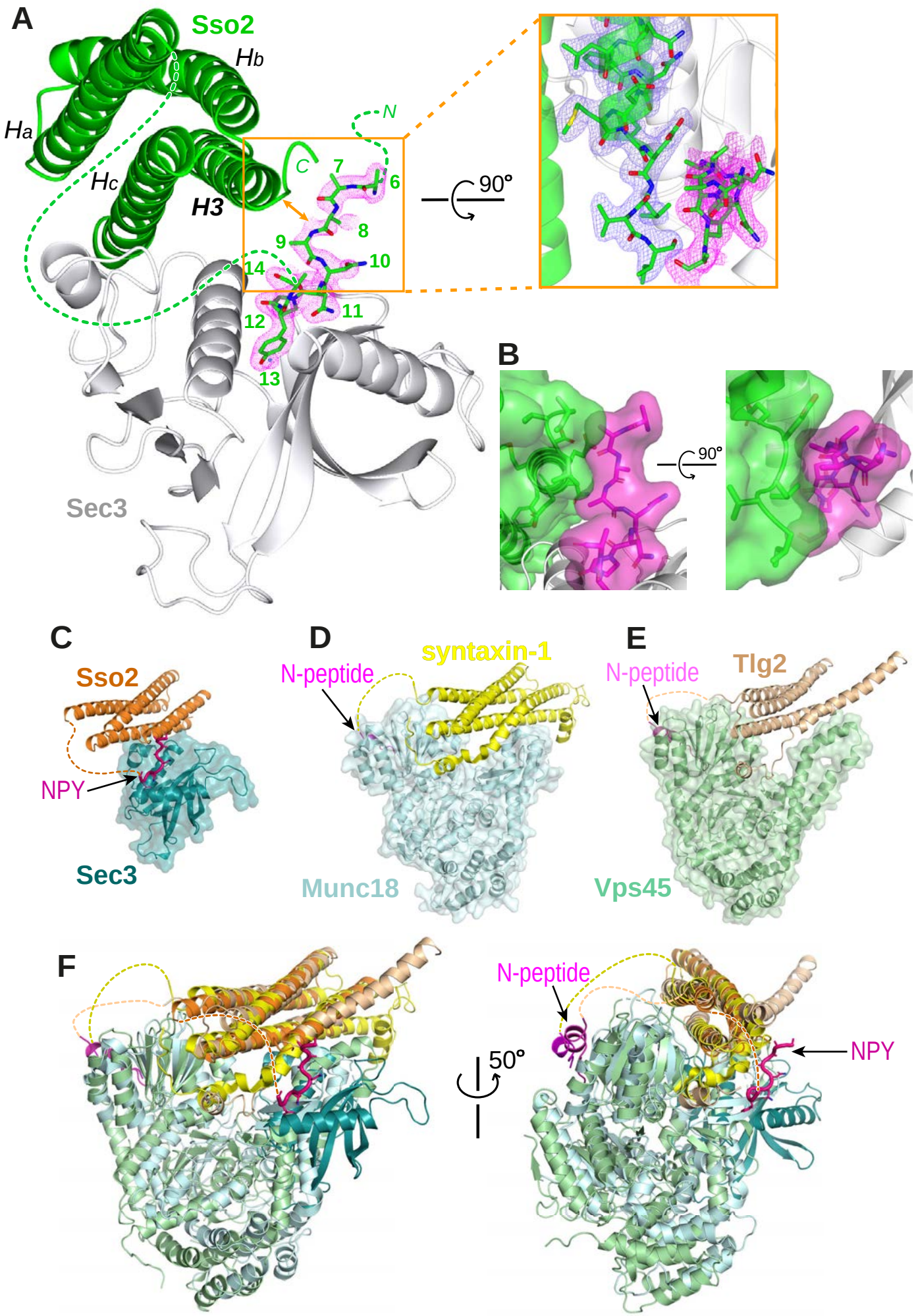
A
Sso2
Hb
Ha
Hc
H3
N
C
7
6
8
9
10
14
11
12
13
90°
Sec3
B
90°
C
Sso2
NPY
Sec3
D
syntaxin-1
N-peptide
Munc18
E
N-peptide
Tlg2
Vps45
F
N-peptide
NPY
50°